Probing Nanoscale Solids at Thermal Extremes

G. E. Begtrup,[1,2] K. G. Ray,[1] B. M. Kessler,[1] T. D. Yuzvinsky,[1,2,3] H. Garcia,[1] and Alex Zettl[1,2,3]

[1]*Department of Physics, University of California at Berkeley, 94720 Berkeley, California, USA*
[2]*Materials Sciences Division, Lawrence Berkeley National Laboratory, 94720 Berkeley, California, USA*
[3]*Center of Integrated Nanomechanical Systems, 94720 Berkeley, California, USA*

(Received 30 April 2007; revised manuscript received 13 June 2007; published 11 October 2007)

We report a novel nanoscale thermal platform compatible with extreme temperature operation and real-time high-resolution transmission electron microscopy. Applied to multiwall carbon nanotubes, we find atomic-scale stability to 3200 K, demonstrating that carbon nanotubes are more robust than graphite or diamond. Even at these thermal extremes, nanotubes maintain 10% of their peak thermal conductivity and support electrical current densities $\sim 2 \times 10^8$ A/cm^2. We also apply this platform to determine the diameter dependence of the melting temperature of gold nanocrystals down to three nanometers.

DOI: 10.1103/PhysRevLett.99.155901 PACS numbers: 65.80.+n, 07.20.Ka, 81.07.−b

The versatility of carbon-carbon bonding underpins a wealth of extraordinary physical properties. Of the two common allotropes of carbon, sp^3-bonded diamond is electrically insulating and displays exceptional hardness and thermal conductivity, but it is metastable and spontaneously reverts to graphite at elevated temperatures [1]. sp^2-bonded graphite is electrically conducting and very stiff in the sheet direction, but it sublimes at temperatures as low as 2400 K [2]. Carbon nanotubes, which can be grown with near atomic perfection, capitalize on the extraordinary strength of the sp^2 hybridized carbon-carbon bond (one of the strongest in nature), and at room temperature exhibit phenomenal electrical and thermal conductivity as well as outstanding mechanical properties. Furthermore, theoretical studies [3] indicate that nanotubes should withstand extreme temperatures, perhaps as high as 4000 K.

Probing the thermal properties of nanoscale systems at very high temperature is technically challenging due to a variety of complications including the breakdown of supporting materials and calibration uncertainties. Something as seemingly straightforward as measuring local temperature becomes problematic on the nanoscale, especially at high temperature. We have developed a thermal test platform capable of operating at extreme temperatures while providing local temperature information with nanoscale resolution. We apply this platform to an investigation of the high-temperature properties of multiwall carbon nanotubes (MWNTs) and probe the limits of nanotube breakdown in vacuum and the thermal conductivity of nanotubes in the extreme high-temperature limit. In addition, we combine this new technique with calibrated MWNT heaters to address the size dependence of the melting point of metallic nanocrystals.

Figure 1 shows a schematic of the thermal test platform in different stages of construction and operation. Figure 1(a) shows an electrically conducting sample mounted on a custom-fabricated thin silicon nitride (Si_3N_4) membrane [4] that is transparent to high energy electrons, allowing real-time observation in a transmission electron microscope (TEM). As shown in Fig. 1(b), a two-dimensional array of single-shot nanoscale thermometers is formed by subsequently depositing metallic nanoparticles onto the sample and membrane. As electrical current is driven through the sample, Joule heating causes the temperature of the sample (and supporting membrane) to increase. The temperature of different portions of the sample is determined locally by observing the onset of local melting and evaporation of the nanoparticle thermometers. Figure 1(c) shows the sample heated with a higher bias. As the temperature continues to increase, the single-shot thermometers show a ''melting front'' receding from the sample and forming a distinctive pattern on the membrane.

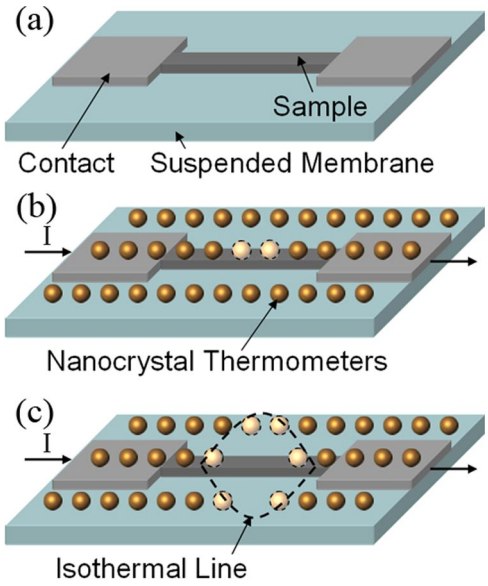

FIG. 1 (color online). Design and operation of the thermal test platform. (a) A nanoscale sample is electrically contacted on a suspended membrane. (b) Nanocrystal thermometers are deposited on the sample. The sample is resistively heated via an electrical current, I, causing the nanocrystals to melt, yielding the temperature of the sample. (c) At higher bias, the melting nanocrystals yield an isothermal line which fans out across the membrane.

This front corresponds to an isothermal line that, by employing finite element analysis to solve the heat distribution profile, can be used to extract the position-dependent temperature along the sample itself. As we demonstrate below, the nanoparticle thermometry method allows not only the local temperature of the sample to be determined (even when it greatly exceeds the melting point of the thermometers), but also its temperature-dependent thermal conductivity.

We apply the thermal measurement platform to MWNTs. Although theoretical studies suggest that nanotubes are surprisingly stable at thermal extremes, the breakdown temperature of MWNTs in vacuum has not been directly determined [5,6] Although the temperature-dependent thermal conductivity κ of MWNTs is well established below room temperature [7], κ in the extreme high-temperature limit remains largely unexplored.

Figure 2 shows a series of TEM images of a MWNT mounted on the thermal test platform, together with nanoparticle thermometers. Small gold nanoparticles (typically <10 nm diameter) comprise a reliable and easy to read local temperature probe since they evaporate immediately upon melting (unlike indium, for example, which has a much lower vapor pressure at melting and electromigrates along nanotubes under similar conditions [8]). Since the melting temperature of gold nanoparticles is diameter dependent, we focus for the moment only on particles with diameter ~ 6 nm, which have a well-established melting temperature of 1275 K [9]. The MWNT sample is electrically contacted using palladium, which yields reliable low-resistance electrical contacts (total sample resistances are typically ~ 10 KΩ in the low bias regime).

Figure 2(a) shows the MWNT device under zero electrical bias conditions. The false color map is derived from finite element analysis described below and here indicates fully isothermal conditions with $T = 300$ K (blue). As the bias is increased, the temperature of the MWNT and membrane increases. Figure 2(b) demonstrates that the MWNT becomes hottest in the center due to the diffusive nature of the electrical conductance in this high bias regime, and the nanoparticle thermometers near the center of the tube are the first to melt and evaporate (the light colored spots on the central part of the membrane are signatures of the evaporated thermometers, not holes in the membrane). As the bias is increased further, the thermometer melting or evaporation front continues to fan out from the center of the nanotube, both along the axis of the nanotube and on the surrounding membrane [Fig. 2(c)]. Eventually, at sufficiently high bias, the Si_3N_4 membrane directly underneath the MWNT becomes so hot that it begins to disintegrate. This disintegration provides a second independent calibration point, at 2173 K, the breakdown temperature of Si_3N_4 [10]. As the bias is still further increased, continued disintegration causes the membrane to peel back from the nanotube, decreasing the heat loss to the substrate and allowing the nanotube to heat even more effectively for a given electrical power input. The MWNT is stable after

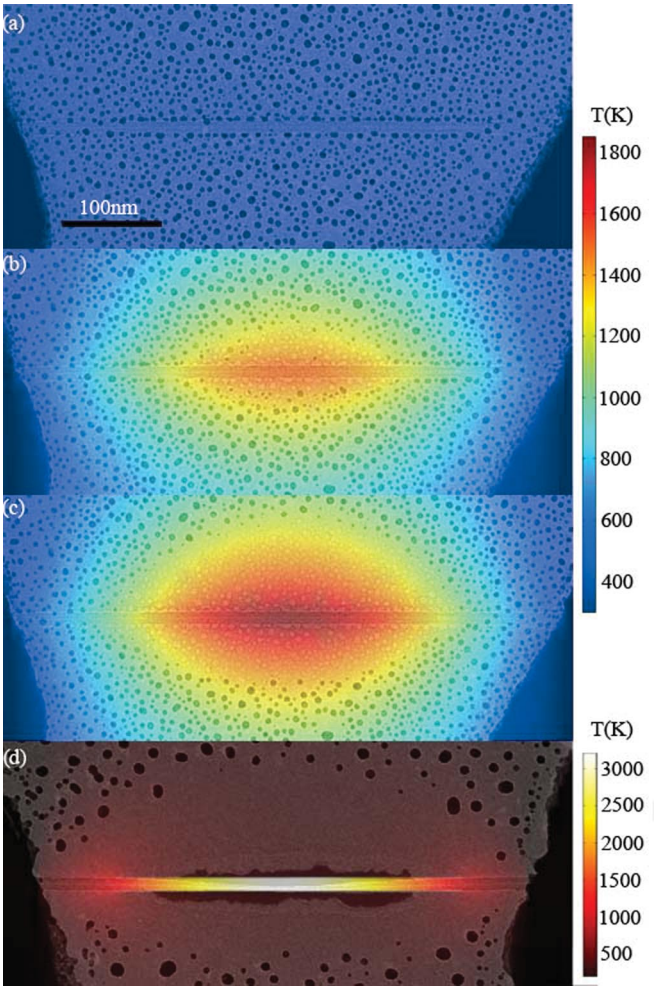

FIG. 2 (color). Operation of MWNT devices. (a)–(d) TEM images of MWNT devices, with color overlays to indicate local temperature [note (d) uses a different color scale]. (a) Zero bias, isothermal ($T = 300$ K) conditions. (b),(c) Same device operating at biases above the threshold for melting of the gold nanoparticles. (d) A different MWNT (chosen for image clarity) operated close to the breakdown temperature of 3200 K. The darker area near the center of the nanotube shows the membrane failure.

suspension under increased bias, immediately indicating survival at temperatures well above that of Si_3N_4. At extreme temperatures the MWNT eventually becomes fully suspended, and ultimately it catastrophically fails. Figure 2(d) shows (for a different MWNT chosen for image clarity) the thermal profile just prior to failure; the center portion of the nanotube is at $T = 3200$ K. Different MWNT devices [including that of Figs. 2(a)–2(c)] typically survive to a similar maximum temperature. The electrical current density prior to failure for the MWNT of Fig. 2(d) (with inner diameter 4.8 nm and outer diameter 14.7 nm) is 1.7×10^8 A/cm^2; other devices show comparable current-carrying capability at the stability threshold.

The local nanotube temperature is determined by applying finite element analysis which requires a discussion of the thermal conductivity of MWNTs. κ for nanotubes

below room temperature has been extensively probed, with measurements [11] and simulations [12] showing an increase in κ with increasing temperature. At high temperatures, increased phonon scattering [10] should cause a decrease in the thermal conductivity with a peak expected near room temperature [7,12,13]. Despite great scientific and practical interest in the high-temperature thermal conductivity of nanotubes, no reliable experiments have been performed in the extreme high-temperature limit.

To determine κ of MWNTs at high temperature, we use the thermal test platform configuration and employ finite element analysis to solve the heat equation at a given applied bias to determine the temperature distribution of the system. As a diffusive conductor in this regime, demonstrated by the shape of the isotherms peaking in the center of the device, the MWNT obeys the classical heat equation with Joule heating. Treating the nanotube as a one-dimensional system with cross-sectional area A yields the heat equation

$$A\nabla(\kappa\nabla T) + (I \cdot V)/L = 0 \quad (1)$$

where κ is the temperature-dependent thermal conductivity, T the temperature, I the electrical bias current, V the voltage across the tube, and L the length of the tube.

We apply Eq. (1) to create a finite element model of the entire system. The thermal and electrical properties of the Si_3N_4 substrate and Pd contacts are known and appropriate boundary conditions are employed. The electrical resistance of the nanotube is experimentally determined. The only free parameter of the system is the temperature-dependent thermal conductivity, $\kappa(T)$. For conditions up to the failure of the Si_3N_4, we self-consistently solve the system for each dissipated power to reproduce the temperature profiles experimentally determined from the nanoparticle thermometers and the breakdown of Si_3N_4. We vary the functional form and value of $\kappa(T)$ to produce a best fit for all dissipated powers of multiple device data. We find that the most appropriate functional form of $\kappa(T)$ in the high-temperature limit incorporates both umklapp and second-order three-phonon processes [14] and is expressed as

$$\kappa(T) = 1/(\alpha T + \beta T^2) \quad (2)$$

with the linear term representing umklapp (two-phonon) scattering and the quadratic term representing 3-phonon processes.

For each device, we determine the fit parameters α and β for the thermal conductivity. For the nanotube shown in Fig. 2(d), we find κ to be 150 W/m K at 1275 K, with $\alpha = 4.8 \times 10^{-6}$ m/W and $\beta = 4.3 \times 10^{-10}$ m/W K. Hence, the contribution of three-phonon scattering modes becomes non-negligible at temperatures exceeding 1100 K.

Once $\kappa(T)$ is known, the system is fully characterized, such that the local temperature can be determined for any given dissipated power. We now apply finite element analysis to determine the nanotube temperature beyond the local failure of the Si_3N_4 membrane. The model is adjusted to reflect the missing center of the membrane with heat still flowing through the remaining edges of the Si_3N_4. We solve the system with the determined $\kappa(T)$ and the measured dissipated power immediately prior to nanotube failure, yielding the measured onset temperature for MWNT sublimation, the highest temperature at the center of the nanotube, to be 3200 K. This temperature approaches theoretical predictions for nanotube stability [3] and is 800 K higher than the onset temperature of sublimation of graphite [2]. Nanotubes are thus the most robust form of carbon. The exceptional mechanical stability is attributed to the strength of the sp^2 bond and the relatively defect-free geometry of MWNTs.

Figure 3 shows the full temperature dependence of $\kappa(T)$ from 10 K to nanotube failure at 3200 K. Low temperature data, up to 410 K, are taken from the literature [15–17]. The solid line shows the high temperature κ obtained from the experiment given by Eq. (2) with parameters α and β obtained above. All values are normalized at 300 K. This curve is representative of all the nanotubes probed in this study. Importantly, at $T \sim 1000$ K the MWNT retains 50% of its peak thermal conductance, and at $T \sim 3000$ K it still displays 10% retention. Even at temperature extremes, MWNTs are impressive thermal conductors.

By using MWNTs as ultra-high-temperature heating elements, our calibrated test platform can probe the high-temperature properties of other nanoscale systems, including nanocrystals of various sizes. The melting point of our gold nanoparticle thermometers is well-established at particle size $d = 6$ nm, but the melting point is known to be highly diameter dependent, a phenomenon first described by Pawlow in 1909 [18]. Surprisingly, the melting point of gold nanoparticles has not been experimentally mapped out in the ultrasmall particle regime [9]. We here determine

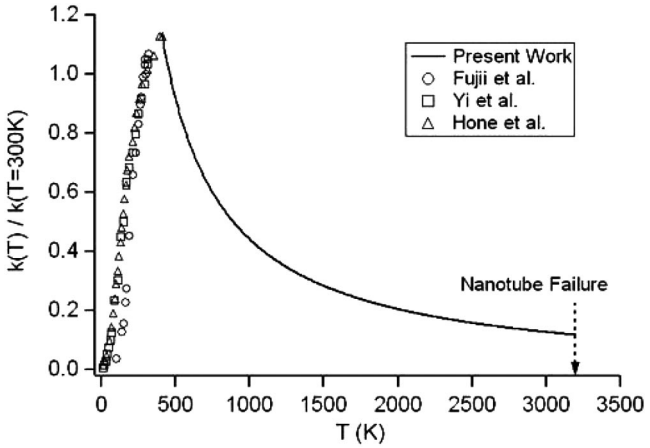

FIG. 3. Full temperature dependence of the thermal conductivity κ of MWNTs. Experimentally determined high-temperature κ reflecting umklapp and three-phonon processes [Eq. (2)] is plotted as a solid line. Also plotted are literature results for κ of various carbon nanotubes at low temperatures [15–17].

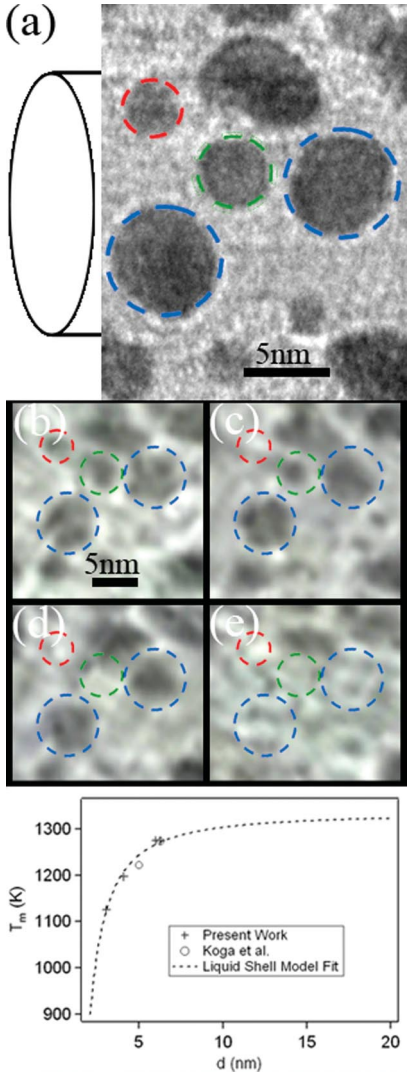

FIG. 4 (color). Diameter (d) dependence of the melting point (T_m) of gold nanoparticles (NPs). Scales are 5 nm (a) TEM image of MWNT heater with NPs (lines indicate MWNT outer wall). Selected NPs on the heater are outlined in color: red ($d = 3$ nm), green ($d = 4$ nm), and blue ($d = 6$, 6.5 nm). (b)–(e) TEM video images as heater bias is increased with rendered models of system. (b) $T = 1165$ K, no NPs have melted. (c) $T = 1130$ K, 3 nm NP melts and evaporates. (d) $T = 1200$ K, 4 nm NP evaporates. (e) $T = 1275$ K, 6, 6.5 nm NPs evaporate. (f) T_m vs d. Data from this study (crosses) show strong diameter dependence, with experimental results of Koga *et al.* (open circles). The liquid shell model (dashed line) provides an excellent fit to the data.

the melting point of gold particles down to 3 nm in diameter.

Figures 4(a)–4(e) show TEM observations of the melting point of gold nanoparticles, employing the calibrated test platform with a MWNT heater. Gold nanoparticles of various sizes reside directly atop the heater. We step the bias applied to the heater and determine the temperature at each steady state plateau. As anticipated, smaller gold nanoparticles melt at lower temperatures due to an enhanced surface-to-volume ratio. Figure 4(f) shows the resulting melting temperature, T_m, as a function of gold nanoparticle diameter d. The dashed line is a fit to the data of the liquid shell model [19] with a shell thickness of 0.5 nm. T_m of gold nanoparticles, and the applicability of the liquid shell model, are thus experimentally established to $d = 3$ nm.

Our thermal test platform has obvious application for the testing of high-temperature properties of a broad range of other nanoscale particles and device structures. Of great practical importance is the unprecedented extreme thermal stability of MWNTs, which surpasses the stability of other forms of carbon. The combination of high strength, high thermal and electrical conductivity, low weight, and exceptional thermal stability presents exciting opportunities for the use of MWNTs under extreme conditions.

[1] T. Evans and P. F. James, Proc. R. Soc. A **277**, 260 (1964).
[2] J. Haines and C. Tsai, *Graphite Sublimation Tests for the Muon-Collider/Neutrino Factory Target Development Program* (U.S. DOE, Oak Ridge, TN, 2002).
[3] Y. Miyamoto, S. Berber, and M. Yoon *et al.*, Physica (Amsterdam) **323B**, 78 (2002).
[4] T. D. Yuzvinsky, W. Mickelson, and S. Aloni *et al.*, Appl. Phys. Lett. **87**, 083103 (2005).
[5] X. Cai, S. Akita, and Y. Nakayama, Thin Solid Films **464–465**, 364 (2004).
[6] J. Y. Huang, S. Chen, and S. H. Jo *et al.*, Phys. Rev. Lett. **94**, 236802 (2005).
[7] P. Kim, L. Shi, and A. Majumdar *et al.*, Phys. Rev. Lett. **87**, 215502 (2001).
[8] B. C. Regan, S. Aloni, and R. O. Ritchie *et al.*, Nature (London) **428**, 924 (2004).
[9] K. Koga, T. Ikeshoji, and K. I. Sugawara, Phys. Rev. Lett. **92**, 115507 (2004).
[10] R. C. Weast (CRC Press, Inc., Boca Raton, FL, 1985).
[11] J. Hone, M. Whitney, and C. Piskoti *et al.*, Phys. Rev. B **59**, R2514 (1999).
[12] M. A. Osman and D. Srivastava, Nanotechnology **12**, 21 (2001).
[13] E. Pop, D. Mann, and Q. Wang *et al.*, Nano Lett. **6**, 96 (2006).
[14] N. Mingo and D. A. Broido, Nano Lett. **5**, 1221 (2005).
[15] J. Hone, M. C. Llaguno, and N. M. Nemes *et al.*, Appl. Phys. Lett. **77**, 666 (2000).
[16] M. Fujii, X. Zhang, and H. Xie *et al.*, Phys. Rev. Lett. **95**, 065502 (2005).
[17] W. Yi, L. Lu, and Z. Dian-lin *et al.*, Phys. Rev. B **59**, R9015 (1999).
[18] P. Pawlow, Z. Physik und Chemie **65**, 545 (1909).
[19] Y. G. Chushak and L. S. Bartell, J. Phys. Chem. B **105**, 11 605 (2001).